

Spacecraft pointing stability constraints and instrument disturbance limits for optical remote sensing satellites

Derrick A. Early^{*a}, Alan D. Reth^b, Otilia I. Rodriguez-Alvarez^c

^aSwales Aerospace, 5050 Powder Mill Road, Beltsville, MD 20705 USA;

^bChesapeake Aerospace, P.O. Box 567, Grasonville, MD 21638 USA;

^cNASA Goddard Space Flight Center, Mail stop 415.0, Greenbelt, MD 20771 USA

ABSTRACT

This paper describes the methodology used to develop the spacecraft pointing stability constraints and instrument disturbance limits for the Geostationary Operational Environmental Satellite (GOES) R series of spacecraft launching on or after 2012. Instrument line of sight stability and control requirements drive the spacecraft pointing stability constraints. In turn, the spacecraft constraints are used to define the instrument disturbance limits. The resulting limits on the spacecraft and instruments are defined in terms of spacecraft pointing error displacement, velocity and acceleration.

Keywords: Jitter; pointing stability; disturbances; dynamics; line of sight control

1. INTRODUCTION

The National Oceanic and Atmospheric Administration (NOAA) has been operating geostationary earth imaging weather satellites since 1975. The next generation of Geostationary Operational Environmental Satellites (GOES) will be the R series launching on or after 2012. In the current plan, GOES-R will support three earth-scanning instruments. One is called the Advanced Baseline Imager (ABI). The other two are part of a Hyper-spectral Environmental Suite (HES). These two HES instruments will perform full Disk Soundings (DS) and Coastal Waters (CW) imaging.¹ At the time this paper was written, the architecture of the space segment of GOES-R was under study. The three earth scanning instruments may all fly on one satellite as shown in Figure 1, or the ABI may fly separately from the HES instruments as shown in Figure 2.

The optical performance requirements of these earth-scanning instruments drive their instrument line of sight (LOS) stability requirements. For the development of the spacecraft pointing stability constraints within this paper, assumptions were made to approximate the spacecraft motion to instrument LOS response functions. Using these response functions, spacecraft pointing stability constraints are derived from the instrument LOS stability requirements. Furthermore, the disturbance sources on the spacecraft must be constrained to allow the spacecraft to meet its derived spacecraft pointing stability requirements.

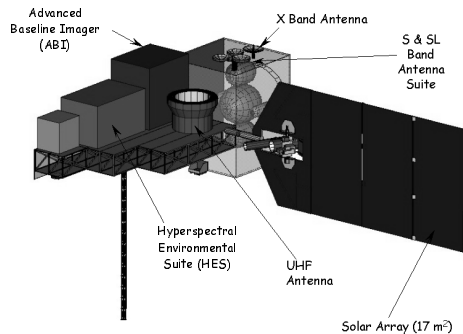


Figure 1: GOES-R single satellite per orbit slot

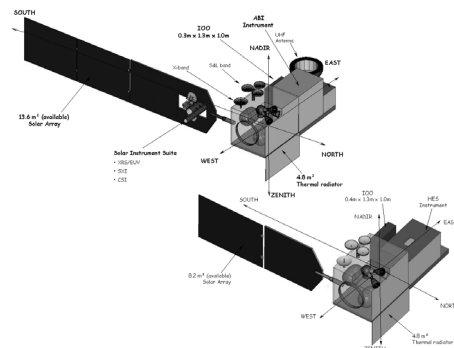


Figure 2: GOES-R multiple satellites per orbit slot

* dearly@swales.com; phone 301 286-4686; facsimile 301 902-4114

The spacecraft disturbance sources include reaction wheels, solar array tracking, and the earth-scanning instruments themselves. A preliminary analysis has shown that the instruments' scan mechanisms are potentially the largest disturbance source on GOES-R.² To limit the instrument disturbances, their contribution to the total spacecraft disturbance will be constrained to some percentage of the derived spacecraft pointing stability requirements.

2. INSTRUMENT LOS REQUIREMENTS

GOES-R imaging systems require LOS stabilization to various peak-to-peak limits, θ_p , over set time periods, τ_w . This limit is expressed in the following inequality constraint.

$$|\theta_l(t) - \theta_l(t + \tau)| \leq \theta_p \text{ for all } \tau \leq \tau_w \quad (1)$$

Table 1 lists estimates for each instrument's LOS limits. The limits defined may be converted to single sinusoidal amplitude limits, θ_A , by the following approximate equations.

$$\theta_A(\omega) = \frac{\theta_p}{2} \text{ if } \omega > \omega_p, \text{ and } \theta_A(\omega) = \frac{\theta_p}{\tau_w \omega} \text{ if } \omega \leq \omega_p \quad (2)$$

where $\omega_p = 2/\tau_w$ and ω is in radians per second. The variable portion of equation (2) results from limiting the rate of a single sine to a maximum of θ_p/τ_w as shown below when $\omega \leq \omega_p$.

$$\dot{\theta} = \frac{\partial}{\partial t} \theta_A(\omega) \sin(\omega t) = \frac{\partial}{\partial t} \frac{\theta_p}{\tau_w \omega} \sin(\omega t) = \frac{\theta_p}{\tau_w} \cos(\omega t) \quad (3)$$

Table 1: Peak to peak instrument pointing limits

i	Instrument	Description	τ_{wi}	θ_{pi} (μrad)
1	ABI	½ km integration	0.8 ms	1.4
2		Swath overlap	30 s	500.0
3	DS	1 km visible integration	2 ms	2.8
4		4 km infrared integration	10 s	11.2
5	CW	Integration ³	88 ms	0.8

3. SPACECRAFT MOTION TO INSTRUMENT LOS RESPONSE

This analysis uses a simple, single axis, two degree-of-freedom (DOF) math model to predict each instrument's LOS motion as a function of the spacecraft motion. Figure 3 illustrates the model used to represent an instrument sensor. This model attempts to represent the first order effects of an instrument like the current GOES imager and sounder.^{4,5} The first DOF, θ_i , is the instrument motion. The second DOF, θ_m , is the mirror motion. For this model, the spacecraft motion, θ_s , is prescribed. All the DOF's are defined with respect to the orbital frame. For this analysis, the orbital frame is assumed to be an inertial frame, although the frame is actually earth pointed. A simple proportional and derivative (PD) controller approximates the servo controller for the scan mirror. The following sections §3.1 through §3.3 develop the response functions for the ABI, DS and CW instruments.

3.1 Spacecraft to ABI LOS

The ABI has a very short integration time listed in Table 1. As a result, this analysis assumes that the ABI LOS will not require active stabilization. The equations of motion for the ABI model may be written as

$$\begin{aligned} J_i \ddot{\theta}_i + c_i (\dot{\theta}_i - \dot{\theta}_s) + c_m (\dot{\theta}_i - \dot{\theta}_m) + k_i (\theta_i - \theta_s) + k_m (\theta_i - \theta_m) &= 0 \\ J_m \ddot{\theta}_m - c_m (\dot{\theta}_i - \dot{\theta}_m) - k_m (\theta_i - \theta_m) &= 0 \end{aligned} \quad (4)$$

where

$$c = 2\zeta\omega J \quad k = \omega^2 J \quad \omega = 2\pi f$$

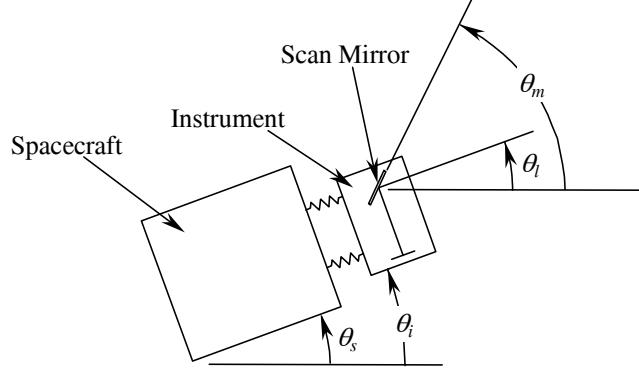


Figure 3: Single axis instrument model

The instrument and mirror inertias are J_i and J_m respectively. The first bending mode frequency of the instrument mounted on the spacecraft is f_i . The scan mirror servo bandwidth is f_m . The viscous damping factors for the instrument and the mirror servo are ζ_i and ζ_m respectively.

Using the Laplace transformation below for the time dependent variables in equation (4)⁶

$$\theta(s) = \int_0^{\infty} e^{-st} \theta(t) dt \quad (5)$$

yields

$$\begin{aligned} J_i s^2 \theta_i + c_i (s \theta_i - s \theta_s) + c_m (s \theta_i - s \theta_m) + k_i (\theta_i - \theta_s) + k_m (\theta_i - \theta_m) &= 0 \\ J_m s^2 \theta_m - c_m (s \theta_i - s \theta_m) - k_m (\theta_i - \theta_m) &= 0 \end{aligned} \quad (6)$$

Collect θ_i and θ_m .

$$\begin{aligned} [J_i s^2 + (c_i + c_m)s + k_i + k_m] \theta_i - (c_m s + k_m) \theta_m &= (c_i s + k_i) \theta_s \\ -(c_m s + k_m) \theta_i + (J_m s^2 + c_m s + k_m) \theta_m &= 0 \end{aligned} \quad (7)$$

Solve for θ_i and θ_m .

$$\theta_i = H_{is} \theta_s \quad (8)$$

$$\theta_m = H_{ms} \theta_s \quad (9)$$

$$H_{is} = (J_m s^2 + c_m s + k_m)(c_i s + k_i) / D \quad (10)$$

$$H_{ms} = (c_m s + k_m)(c_i s + k_i) / D \quad (11)$$

$$D = (J_m s^2 + c_m s + k_m)[J_i s^2 + (c_i + c_m)s + k_i + k_m] - (c_m s + k_m)^2 \quad (12)$$

The LOS of the instrument for both the east-west (EW) and north-south (NS) axes as function of the mirror and instrument angles and may be approximated by

$$\theta_l = k_c \theta_m + (1 - k_c) \theta_i \quad (13)$$

where $k_c = 2$ for EW or $k_c = 1$ for NS. Now the LOS can be related to the spacecraft motion.

$$\theta_{l,abi} = H_{ls,abi} \theta_s \quad (14)$$

$$H_{ls,abi} = k_c H_{ms} + (1 - k_c) H_{is} \quad (15)$$

Using the parameters listed in Table 2 and equation (14), frequency response functions were computed for the spacecraft motion to instrument LOS for both EW and NS. Figure 4 plots the results.

Table 2: Math model parameters

Parameter	Value		Units
	EW	NS	
J_i	37.5	22.0	kg-m ²
f_i	25	25	Hz
ζ_i	5	5	%
J_m	0.25	0.5	kg-m ²
f_m	20	20	Hz
ζ_m	70.7	70.7	%

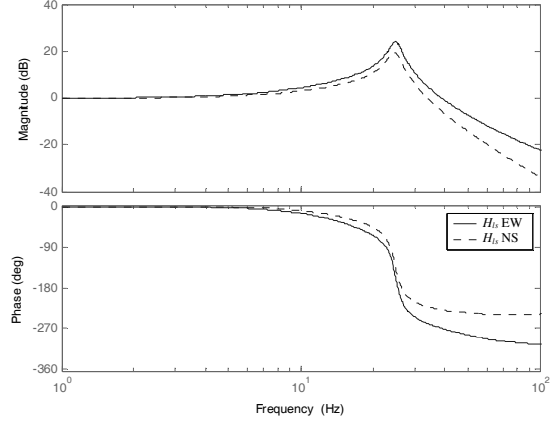


Figure 4: Spacecraft motion to ABI instrument LOS response

3.2 Spacecraft to DS LOS

The DS has a longer integration time than the ABI. As a result, this analysis assumes that the spacecraft motion will be measured and steered out by the DS instrument. To model this, a commanded scan mirror angle term, θ_c , is added to equation (4).

$$J_i \ddot{\theta}_i + c_i (\dot{\theta}_i - \dot{\theta}_s) + c_m (\dot{\theta}_i - \dot{\theta}_m + \dot{\theta}_c) + k_i (\theta_i - \theta_s) + k_m (\theta_i - \theta_m + \theta_c) = 0 \quad (16)$$

$$J_m \ddot{\theta}_m - c_m (\dot{\theta}_i - \dot{\theta}_m + \dot{\theta}_c) - k_m (\theta_i - \theta_m + \theta_c) = 0$$

Taking the Laplace transformation and solving for θ_i and θ_m yields the following equations.

$$\theta_i = H_{is} \theta_s + H_{ic} \theta_c \quad \theta_m = H_{ms} \theta_s + H_{mc} \theta_c \quad (17)$$

$$H_{ic} = [(c_m s + k_m)^2 - (J_m s^2 + c_m s + k_m)(c_m s + k_m)] / D \quad (18)$$

$$H_{mc} = \{ [J_i s^2 + (c_i + c_m)s + k_i + k_m](c_m s + k_m) - (c_m s + k_m)^2 \} / D \quad (19)$$

The spacecraft motion will be measured by the attitude and control system (ACS) gyros as represented by H_{gs} . This measurement will have both phase lag and latency. A 2nd order low-pass filter models the gyro phase lag as represented by H_{gd} , and a 2nd order Pade approximation models the gyro latency as represented by H_{ds} .⁷

$$\theta_g = H_{gs} \theta_s \quad H_{gs} = H_{gd} H_{ds} \quad (20)$$

$$H_{gd} = \omega_g^2 / (s^2 + 2\zeta_g \omega_g s + \omega_g^2) \quad \omega_g = 2\pi f_g \quad (21)$$

$$H_{ds} = (\tau_d^2 s^2 - 6\tau_d s + 12) / (\tau_d^2 s^2 + 6\tau_d s + 12) \quad (22)$$

The spacecraft motion as measured by the gyro, θ_g , is scaled by the following to get the commanded mirror angle, θ_c .

$$\theta_c = \theta_g / k_c \quad (23)$$

Now the DS LOS can be related to the spacecraft motion by using (13), (15), (17), (20) and (23).

$$\theta_{l,ds} = H_{ls,ds} \theta_s \quad (24)$$

$$H_{ls,ds} = H_{ls,abi} - [k_c H_{mc} + (1 - k_c) H_{ic}] H_{gd} H_{ds} / k_c \quad (25)$$

Using the parameters listed in Table 3 and equation (24), frequency response functions were computed for the spacecraft motion to the DS instrument LOS for both EW and NS. Figure 5 plots the results.

Table 3: Gyro model parameters

Parameter	Value	Units
f_g	25	Hz
ζ_g	70.7	%
τ_d	7	ms

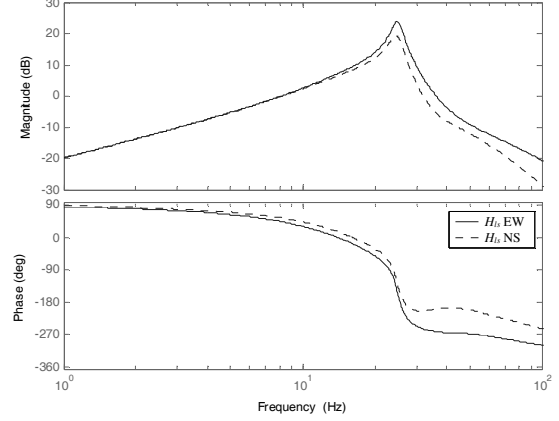


Figure 5: Spacecraft motion to DS instrument LOS response

3.3 Spacecraft to CW LOS

The CW instrument has both a long integration time and tight pointing requirements. To avoid over constraining the spacecraft motions, this analysis assumes that the CW will use a fast steering mirror (FSM). Unlike the previous DS instrument, the scan mirror servo is not used here to stabilize its LOS. Only the FSM is used. As a result, any scan mirror servo errors need to be included in the command to the FSM. The FSM is modeled with a simple PD controller, and it is assumed to be free of reactions. The transfer function for the FSM is

$$\theta_f = H_{fc}\theta_c \quad (26)$$

$$H_{fc} = \frac{2\zeta_f\omega_f s + \omega_f^2}{s^2 + 2\zeta_f\omega_f s + \omega_f^2} \quad \omega_f = 2\pi f_f \quad (27)$$

Assuming an optical gain of k_f , the CW LOS is a function of the spacecraft motion and the FSM commanded angle.

$$\theta_{l,cw} = H_{ls,abi}\theta_s - k_f H_{fc}\theta_c \quad (28)$$

To control the FSM, a high bandwidth angular displacement sensor (ADS) measures the motion of the instrument. This sensor is modeled with a high pass and a low pass second order filter in series.⁸

$$\theta_a = H_{ai}\theta_i \quad H_{ai} = H_{al}H_{li} \quad (29)$$

$$H_{al} = s^2 / (s^2 + 2\zeta_h\omega_h s + \omega_h^2) \quad \omega_h = 2\pi f_h \quad (30)$$

$$H_{li} = \omega_l^2 / (s^2 + 2\zeta_l\omega_l s + \omega_l^2) \quad \omega_l = 2\pi f_l \quad (31)$$

Since the ADS does not measure low frequency motions, a complementary filter must be made to merge the ADS and the gyro measurements. This filter is modeled with the following transfer function.

$$\bar{\theta}_c = H_{cg}\theta_g \quad H_{cg} = (1 - H_{al})H_{cl} / H_{gd} \quad (32)$$

$$H_{cl} = \omega_c^2 / (s^2 + 2\zeta_c\omega_c s + \omega_c^2) \quad \omega_c = 2\pi f_c \quad (33)$$

The scan mirror servo error is modeled as the following.

$$\varepsilon_{mi} = \theta_m - \theta_i \quad (34)$$

To minimize the LOS motion, the FSM commanded angle is defined as the following function of the complimentary gyro signal, the ADS signal and the scan mirror servo error.

$$\theta_c = (\bar{\theta}_c + \theta_a + k_c \varepsilon_{mi}) / k_f \quad (35)$$

Now the CW LOS is related to the spacecraft motion by the following transfer function.

$$\theta_{l,cw} = H_{ls,cw} \theta_s \quad (36)$$

$$H_{ls,cw} = H_{ls,abi} - H_{fc} [H_{cg} H_{gs} + H_{ai} H_{is} + k_c (H_{ms} - H_{is})] \quad (37)$$

Using the parameters listed in Table 4 and equation (36), frequency response functions were computed for the spacecraft motion to the CW instrument LOS for both EW and NS. Figure 6 plots the results.

Table 4: CW model parameters

Parameter	Value	Units
f_f	150	Hz
f_l	0.8	Hz
f_h	1500	Hz
f_c	50	Hz
$\zeta_f, \zeta_l, \zeta_h, \zeta_c$	70.7	%

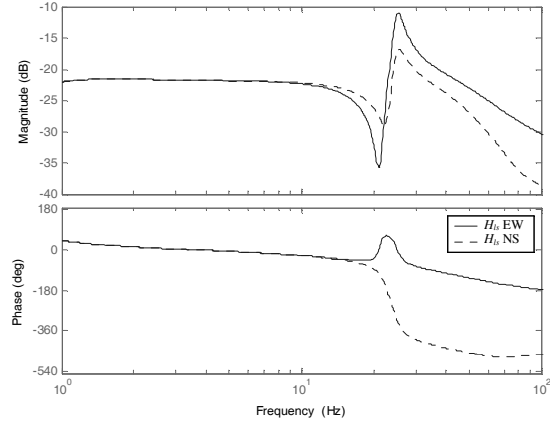


Figure 6: Spacecraft motion to CW instrument LOS response

4. INSTRUMENT TORQUE TO SPACECRAFT MOTION RESPONSE

In this analysis, the instrument torque to spacecraft motion response functions are derived from a simple finite element math model of an assumed GOES-R spacecraft that includes a solar array, magnetometer boom and an optical bench as shown in Figure 7.⁹ The bus was constrained in roll, pitch and yaw by soft springs tuned to 0.01 Hz to represent the proportional part of spacecraft attitude control. The resulting rigid-body modes for roll, pitch and yaw are damped at 30% to represent the derivative part of spacecraft control. The solar array modes that are less than 1 Hz will be passively damped at 2%. The remaining structural modes are damped at 0.1%. The assumed mass properties for the model are listed in Table 5.

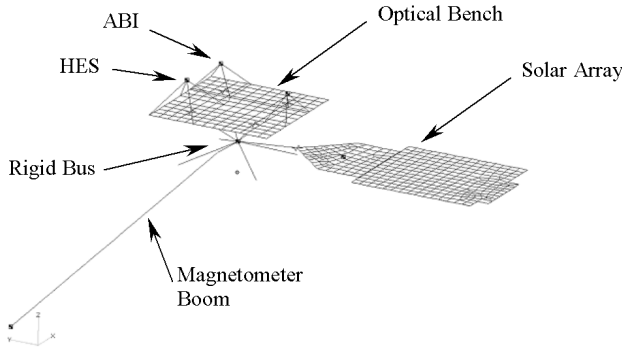


Figure 7: Spacecraft model

Table 5: Spacecraft model mass properties

Property	Value	Units
m	2055	kg
I_{xx}	4620	kg-m ²
I_{yy}	3246	kg-m ²
I_{zz}	4836	kg-m ²

4.1 Math model reduction

The equation of motion for the spacecraft math model may be written as

$$M\ddot{x} + C\dot{x} + Kx = F \quad (38)$$

where M , C and K are constant mass, damping and stiffness matrices respectively. x is a vector of perturbations or small displacements within the spacecraft body frame, and x is a function of time. F is a vector of time dependent forces applied at each degree of freedom. Using the transformation $x = \Phi \xi$, equation (38) becomes

$$\ddot{\xi} + 2Z\Lambda^{1/2}\dot{\xi} + \Lambda\xi = \Phi^T F \quad (39)$$

Where Λ is a diagonal matrix of the eigenvalues, λ_i , and Φ is a matrix of eigenvectors, ϕ_i . The eigenvalues and eigenvectors must nontrivially solve the following

$$M\phi_i\lambda_i = K\phi_i \quad \text{with} \quad \Phi^T M\Phi \equiv I \quad (40)$$

To decouple the ordinary differential equations in equation (39), the matrix Z is assumed to be a diagonal matrix of viscous damping factors, ζ_j . Selecting a particular location, i , for the excitation force and using the decoupled damping assumption, equation (39) becomes

$$\ddot{\xi}_j + 2\zeta_j\omega_j\dot{\xi}_j + \omega_j^2\xi_j = \phi_{ij}f_i \quad (41)$$

Using a Laplace transformation and solving for ξ_j of equation (41) becomes

$$\xi_j = H_{\xi_j f_i} f_i \quad \text{where} \quad H_{\xi_j f_i} = \phi_{ij} / (s^2 + 2\zeta_j\omega_j s + \omega_j^2) \quad (42)$$

Now to obtain the response of a particular degree of freedom, x_o , within vector x , use

$$x_o = \Phi_o \xi \quad (43)$$

$$x_o = \sum_j \phi_{oj} \xi_j \quad (44)$$

Substitute equation (42). Define $\theta_s \equiv x_o$ and $T \equiv f_i$, and substitute i for j .

$$\theta_s = H_{st} T \quad (45)$$

$$H_{st} = \sum_{i=1}^n \frac{1/J_i}{s^2 + 2\zeta_i\omega_i s + \omega_i^2} \quad \text{where} \quad J_i = 1/\phi_{si}\phi_{ti} \quad \text{and} \quad \omega_i = 2\pi f_i \quad (46)$$

and n is the total number of eigenvalues used.

4.2 Math model reduction results

Tables 6 through 8 list the parameters for equation (46) for the spacecraft roll, pitch and yaw reduced from the spacecraft finite element math model. Rows with large J values were eliminated to further simplify the reduced model. Figure 8 plots the instrument torque to spacecraft motion response functions. These response functions will be used below to constrain the instrument torques.

Table 6: Parameters for roll torques about the x-axis

i	f_i (Hz)	ζ_i (%)	J_i (kg-m ²)
1	0.01	30.0	4721
2	0.40	2.0	10733
3	1.34	0.1	59081
4	1.92	0.1	34514
5	13.24	0.1	972
6	16.54	0.1	732
7	23.56	0.1	3468
8	30.55	0.1	5017
9	30.91	0.1	2975
10	31.00	0.1	1313
11	31.17	0.1	1204
12	39.36	0.1	25821

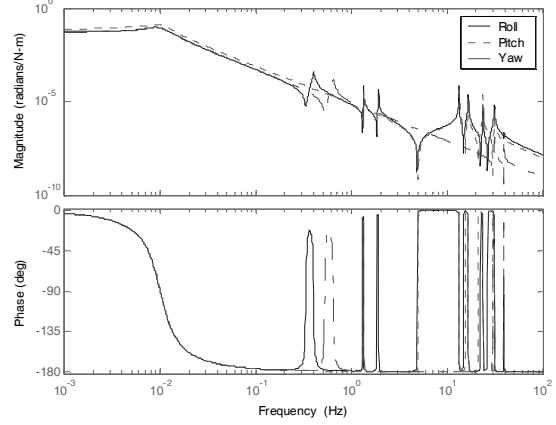


Figure 8: Instrument torque to spacecraft motion response functions

Table 7: Parameters for pitch torques about the y-axis

i	f_i (Hz)	ζ_i (%)	J_i (kg-m ²)
1	0.01	30.0	3203
2	1.35	0.1	89061
3	13.24	0.1	820
4	16.54	0.1	1620
5	23.56	0.1	985
6	30.55	0.1	55722
7	30.91	0.1	8377
8	31.00	0.1	3897
9	31.17	0.1	6104

Table 8: Parameters for yaw torques about the z-axis

i	f_i (Hz)	ζ_i (%)	J_i (kg-m ²)
1	0.01	30.0	4873
2	0.64	2.0	10001
3	1.35	0.1	76471
4	31.00	0.1	45578
5	39.36	0.1	73013

5. SPACECRAFT MOTION CONSTRAINTS

This section develops the spacecraft motion constraints derived from the instrument LOS stability requirements listed in Table 1 using the instrument LOS response functions defined in §3.1 through §3.3 above. Each instrument has a spacecraft motion to LOS response function.

$$\theta_l = H_{ls} \theta_s \quad (47)$$

In order to meet the LOS stability requirements, the LOS needs to be constrained to be less than equation (2).

$$\theta_l < \theta_A \quad (48)$$

Substituting equation (47) into (48) and solving for the spacecraft motion constraint yields.

$$\theta_s < H_{ls}^{-1} \theta_A \quad (49)$$

Using the instrument LOS limits from Table 1 and equations (2), (14), (24), (36) and (49), Figures 9 through 11 plot θ_A and θ_s curves for the ABI, DS and CW instruments respectively. Figure 12 overlays the spacecraft motion constraints for the instruments, and it plots the spacecraft motion constraint envelope listed in Table 9. The limits defined in Table 9 were chosen to envelope the spacecraft motion limits for all three instruments while allowing for reasonable variations in the parameters used in the instrument LOS response functions.

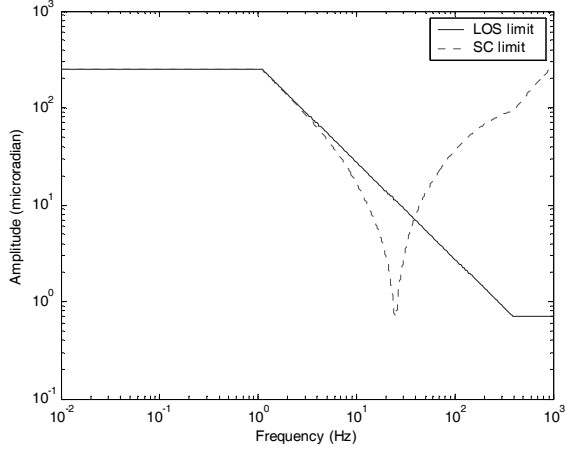


Figure 9: ABI LOS (solid) and spacecraft stability constraints (dashed)

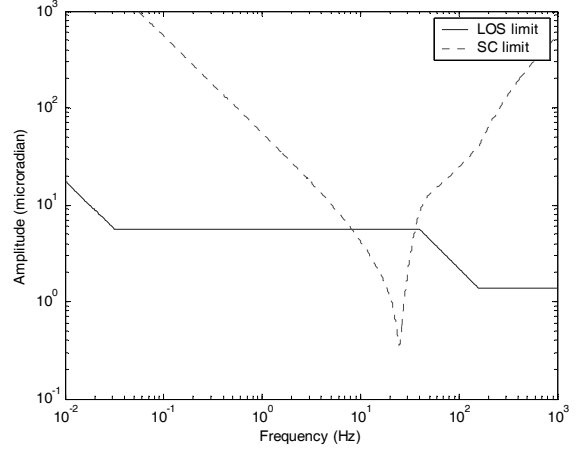


Figure 10: DS LOS (solid) and spacecraft stability constraints (dashed)

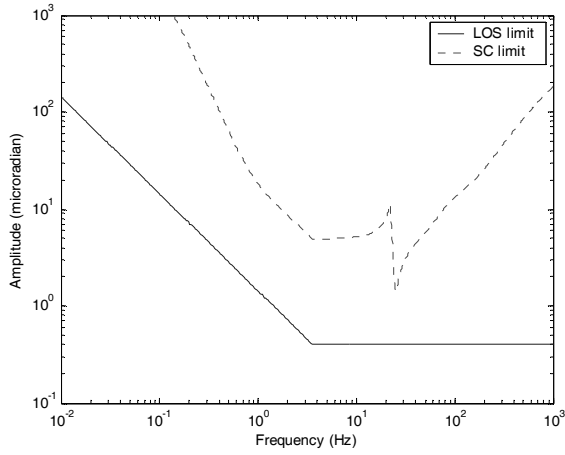


Figure 11: CW LOS (solid) and spacecraft stability constraints (dashed)

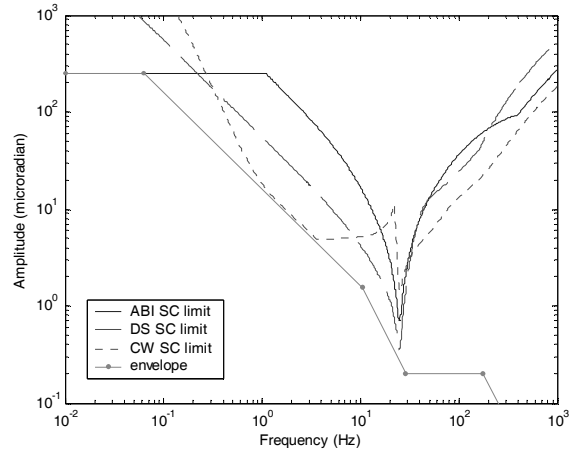


Figure 12: ABI (solid line), DS (large dash line), CW (fine dash line) and envelope (solid line with dots) spacecraft stability constraints

Table 9: Spacecraft motion constraint envelope

i	f_{ei} (Hz)	θ_{ei} (μrad)	$\dot{\theta}_{ei}$ ($\mu\text{rad/s}$)	$\ddot{\theta}_{ei}$ (mrad/s^2)
1	0.010	250	16	0.0
2	0.0636	250	100	0.0
3	10.46	1.52	100	6.6
4	28.85	0.20	36	6.6
5	176.3	0.20	222	245
6	500.0	0.0248	78	245

The frequency domain constraints defined in Table 9 can be used to constrain the time domain motion responses of the spacecraft by the following five inequality equations.

$$|\theta_s| < \theta_{e1}, \quad |\dot{\theta}_{s2}| < \dot{\theta}_{e2}, \quad |\ddot{\theta}_{s3}| < \ddot{\theta}_{e3}, \quad |\theta_{s4}| < \theta_{e4} \quad \text{and} \quad |\ddot{\theta}_{s5}| < \ddot{\theta}_{e5} \quad (50)$$

where

$$\theta_{si} = k_i H_i \theta_s \quad (51)$$

$$k_i = 1 / \min \arg(|H_i(\omega_{ei})|, |H_i(\omega_{ei+1})|) \quad (52)$$

$$\omega_{ei} = 2\pi f_{ei} \text{ and } i=2,3,4 \text{ and } 5 \quad (53)$$

The five inequality constraints in equation (50) represent the five logarithmic linear segments of the spacecraft displacement envelope plotted in Figure 12. H_i is a band pass filter passing signals with frequencies between f_{ei}/α and αf_{ei+1} . The parameter α was selected so that k_i was less than 105%.

6. INSTRUMENT DISTURBANCE CONSTRAINTS

This section develops instrument torque constraints. Instrument torques are constrained indirectly here by constraining the spacecraft motion induced by the instrument torques. The instrument torque to spacecraft motion response functions were develop above in §4. A percentage of the spacecraft motion constraint envelope defined in Table 9 is allocated for each instrument as defined by equation (54) and Table 10. The allocations for the HES instruments, DS and CW, combined are the same as the ABI. These two instruments may be combined into a single instrument that performs both functions. In that case, the allocations would combine for a total of 40% for the DS plus CW instrument.

$$\theta_s < \beta_j \theta_e \quad (54)$$

Substituting into equation (50) into (54) yields five inequality constraints for each of the instruments.

$$|\theta_s| < \beta_j \theta_{e1}, \quad |\dot{\theta}_{s2}| < \beta_j \dot{\theta}_{e2}, \quad |\ddot{\theta}_{s3}| < \beta_j \ddot{\theta}_{e3}, \quad |\theta_{s4}| < \beta_j \theta_{e4} \text{ and } |\ddot{\theta}_{s5}| < \beta_j \ddot{\theta}_{e5} \quad (55)$$

The spacecraft motions induced by the instrument are computed by filtering the instrument torques with H_{st} from equation (46). These motions induced by the instrument must comply with the inequality constraints in equation (55).

Table 10: Instrument disturbance allocations

j	Instrument	β_j (%)
1	ABI	40
2	DS	20
3	CW	20

7. PREDICTED ABI INDUCED SPACECRAFT MOTIONS

This section shows predictions for the ABI induced spacecraft motions over a 15 minute period. Figure 13 plots a representative ABI scan schedule simulation. This 15 minute schedule includes mesoscale (1000 km x 1000 km) scans every 30 s, contiguous United States (CONUS) scans every 5 minute, star sightings every minute, one full earth disk scan and one black body calibration slew. Figure 14 plots the predicted roll torque required for this scan using the assumed NS scanner inertia, J_m , from Table 2.

Tables 11 and 12 list the ABI induced absolute peak spacecraft responses for roll and pitch. All of the responses were well within the limits defined in §6 for the ABI instrument. Since the ABI meets its limits, it should be compatible with itself and the DS and CW. Figure 15 plots the predicted ABI induced spacecraft roll time history. Figure 16 plots the predicted ABI induced spacecraft roll rate filtered with a 12 order Butterworth using 0.06 and 11.5 Hz as the minus 3 dB response frequencies.

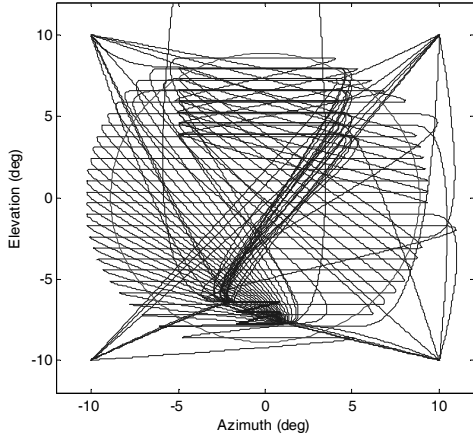


Figure 13: ABI LOS scan pattern

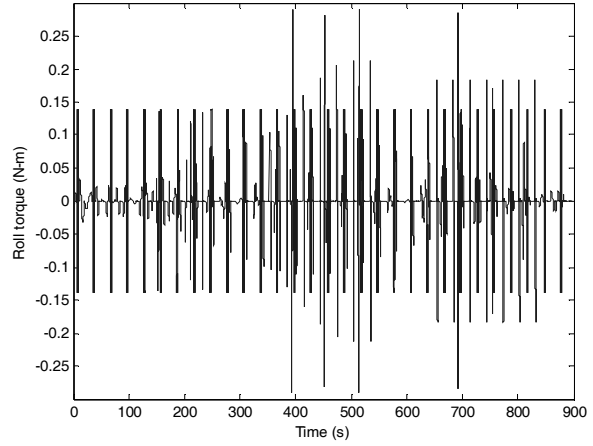


Figure 14: ABI roll torque time history

Table 11: ABI induced spacecraft roll responses

Response	Peak	Limit	Units
$ \theta_s $	77	100	(μrad)
$ \dot{\theta}_{s2} $	30	40	($\mu\text{rad/s}$)
$ \ddot{\theta}_{s3} $	0.2	2.6	(mrad/s^2)
$ \theta_{s4} $	3.7	80	(nrad)
$ \ddot{\theta}_{s5} $	0.0	98	(mrad/s^2)

Table 12: ABI induced spacecraft pitch responses

Response	Peak	Limit	Units
$ \theta_s $	10	100	(μrad)
$ \dot{\theta}_{s2} $	14	40	($\mu\text{rad/s}$)
$ \ddot{\theta}_{s3} $	0.2	2.6	(mrad/s^2)
$ \theta_{s4} $	1.6	80	(nrad)
$ \ddot{\theta}_{s5} $	0.0	98	(mrad/s^2)

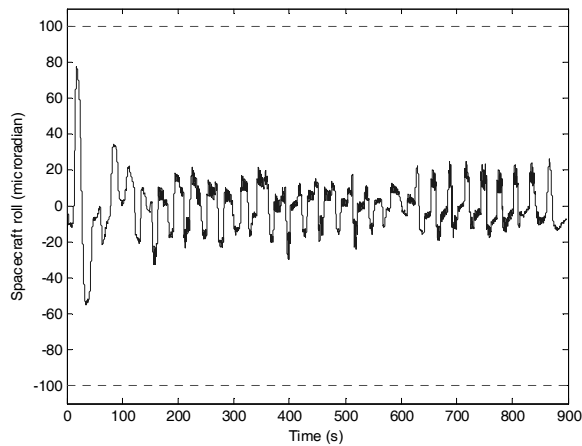


Figure 15: ABI induced spacecraft roll (solid) and limit (dash)

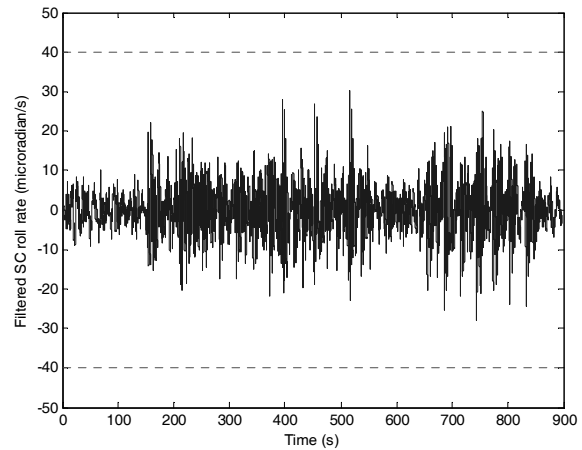


Figure 16: Filtered ABI induced spacecraft roll rate from 0.06 to 11.5 Hz (solid) and limit (dash)

8. CONCLUSIONS

Constraints for the spacecraft motions were developed for the GOES-R spacecraft. As long as the spacecraft motions are compliant with these constraints, the earth scanning instruments should be able to meet their LOS stability requirements. Unfortunately, the instruments themselves are most likely to cause the spacecraft to violate its motion constraints. Therefore, the spacecraft motions induced by the instruments were constrained by an allocation of the total allowed. This indirectly constrains the torque produced by the instruments. The instrument induced motion constraints appear to be reasonable, since the predictions of spacecraft motions for the ABI scans of the earth are compliant.

Further study of the spacecraft constraint is needed to determine if its allocation is sufficient to allow for solar array tracking, reaction wheels, thermal distortions and other sources. The constraints for the DS and CW need verification to determine if they can meet their coverage requirements. As an option, torque compensation methods may be required to maintain the pointing stability of the spacecraft.¹⁰

The assumed models need to include sensor and system noise effects and should be refined to improve prediction accuracy. Instrument math model to spacecraft math model coupling should use the component mode substitution method developed by Messrs. Benfield and Hruda.¹¹ The impact of the mission architecture chosen needs review. A single satellite reduces the allocations for each of the instruments, but it has a larger inertia to react the instrument torques. Multiple satellites allow for larger spacecraft motion constraints for the ABI satellite, and larger disturbance allocations for the HES instruments.

ACKNOWLEDGMENTS

This paper and analysis were supported under contract NAS5-01090 with NASA Goddard Space Flight Center. The authors are thankful to Sandra Cauffman, GOES-R Deputy Project Manager, for encouraging the publication of this work. The authors are also very appreciative of the wonderful support from our GOES-R team.

REFERENCES

1. NOAA's Mission Requirements Document I (MRD-I) for the GOES-R Series, Version 0.7, 6 December 2002.
2. W. Haile, "GOES-R Preliminary Jitter Analysis", SAI-TM-1932, Swales Aerospace, 25 March 2002.
3. J.C. Bremer, "HES Coastal Zone Timeline", memorandum, Swales Aerospace, 5 May 2003.
4. *GOES I-M Data Book*, Space Systems Loral, 31 August 1996.
5. *GOES N-Q Data Book*, Boeing Satellite Systems, 2000.
6. L. Meirovitch, *Elements of Vibration Analysis*, McGraw-Hill, New York, 1975, p. 81.
7. G.H. Golub and C.F. Van Loan, *Matrix Computations*, Johns Hopkins University Press, Baltimore, 1989, pp. 557-558.
8. D. Laughlin and D. Smith, "Development and performance of an angular vibration sensor with 1-1000 Hz bandwidth and nanoradian-level noise", *Free-Space Laser Communication and Laser Imaging*, D.G. Voelz and J.C. Ricklin, eds., SPIE, San Diego, 2002, pp. 208-214.
9. J. Shaw, "GOES On-Orbit Model Report", SAI-TM-2024, Swales Aerospace, 19 March 2002.
10. D.A. Early and A.D. Reth, "GOES-R INR Instrument Disturbance Trade", memorandum, SAI-TM-1935, Swales Aerospace, 15 November 2001.
11. W.A. Benfield and R.F. Hruda, "Vibration Analysis of Structures by Component Mode Substitution", *AIAA Journal*, Vol. 9, No. 7, July 1971, pp. 1255-1261.